Torben Kodanek[a], Axel Freytag[a], Anja Schlosser, Suraj Naskar, Thomas Härtling, Dirk Dorfs[a,*] and Nadja Carola Bigall[a,*]

Macroscopic Aerogels with Retained Nanoscopic Plasmonic Properties

https://doi.org/10.1515/zpch-2017-1045
Received October 11, 2017; accepted December 21, 2017

Abstract: Aerogels can bridge the nanoscopic to the macroscopic world. One physical phenomenon typically limited to the nanoscopic world is the occurrence of localized surface plasmon resonances (LSPRs), which are observed in conductive nanoparticles. Once brought into close contact, assemblies or superstructures of these nanoparticles often lose their plasmonic properties in the transition stage towards the bulk material. Therefore, LSPRs are typically not observed in macroscopic objects. The present work aims at voluminous nanoparticle-based aerogels with optical properties close to that of the initial colloidal solution and the possibility to manipulate the final plasmonic properties by bringing the particles into defined distances. In detail, Ag nanocrystals with silica shells ranging from 0 to 12 nm are employed as building blocks, which are assembled from their solution into macroscopic three-dimensional superstructures by freezing and subsequent lyophilization. These cryogelated aerogels are synthesized as monoliths and thin films in which the Ag nanocrystals are arranged in defined distances according to their silica shell. The resulting aerogels exhibit plasmonic properties ranging from a behavior similar to that of the building blocks for the thickest shell to a heavily distorted behavior for bare Ag nanocrystals.

Keywords: aerogels; core-shell heterostructures; plasmon coupling; silver nanoparticles.

[a]**Torben Kodanek, Axel Freytag, Dirk Dorfs and Nadja Carola Bigall:** These authors contributed equally to this work.

***Corresponding authors: Dirk Dorfs and Nadja Carola Bigall,** Institute of Physical Chemistry and Electrochemistry (PCI), Leibniz Universität Hannover, Callinstraße 3A, 30167 Hannover, Germany; and Laboratory for Nano and Quantum Engineering (LNQE), Leibniz Universität Hannover, Schneiderberg 39, 30167 Hannover, Germany, e-mail: dirk.dorfs@pci.uni-hannover.de (D. Dorfs); nadja.bigall@pci.uni-hannover.de (N. C. Bigall)

Torben Kodanek, Axel Freytag, Anja Schlosser and Suraj Naskar: Institute of Physical Chemistry and Electrochemistry (PCI), Leibniz Universität Hannover, Callinstraße 3A, 30167 Hannover, Germany; and Laboratory for Nano and Quantum Engineering (LNQE), Leibniz Universität Hannover, Schneiderberg 39, 30167 Hannover, Germany

Thomas Härtling: Fraunhofer Institute for Ceramic Technologies and Systems IKTS, Maria-Reiche-Str. 2, 01109 Dresden, Germany

1 Introduction

Optical properties of nanoparticles have raised a considerable amount of interest in the last years. While the effects of e.g. localized surface plasmon resonances (LSPRs) are known and researched for more than 100 years [1, 2], a fundamental understanding of the physics behind them was only obtained in the past two decades [3–5]. Nanochemistry utilized this knowledge for modifying the optical properties of materials by two complementary routes. The first route is to synthesize tailor-made nanoparticles by chemically controlling their composition, size and shape [6–9]. Following this route allows to modify the optical properties to a large extent (e.g. the spectral position of the LSPR) [10, 11]. The second route is the assembly of nanoparticles into arrays or self-assembled ordered structures, and exploiting interparticle interactions like plasmon coupling [3, 5, 12–16]. Typically, both methods need to be combined when it comes to utilization of nanomaterials in applications like sensing, spectroscopy or in (photo)catalysis [14, 15, 17, 18]. However, the possibilities of assembling colloidal nanoparticles are insufficient, especially in terms of controlling optical properties of the resulting macroscopic objects. Literature describes various methods for one- and two-dimensional assemblies [3, 12, 13, 19]. Up to now there is no satisfying procedure to build voluminous macroscopic structures while retaining control on the plasmonic properties. Yet, one possible method to retain the nanoparticle properties and exploit interparticle interactions can be aerogel formation [20, 21]. In principle there are two different methods to create these highly voluminous and porous systems. On the one hand aerogels can be produced by supercritical drying of previously created hydrogels. In this regard hydrogels of metal oxides or polymers are often obtained via sol-gel processes as developed by Kistler [22] and further developed by others in the subsequent decades [23]. Another developed approach to gelate nanocrystals of different materials in aqueous solutions bases on the adjustment of the surface chemistry [24–29]. However, the hydrogelation is time consuming and has limitations in organizing the nanoparticles (e.g. 1- or 2-dimensional arrangement cannot be formed) resulting in a random network. Furthermore, hydrogelation via surface chemistry has to be adapted individually for different particles with different surface chemistry. Alternatively, cryogelation as a route to aerogels was recently published, and is based on freezing aqueous colloidal nanoparticle solutions in liquid nitrogen and freeze dry them [30]. Cryogelated aerogels are fabricated much faster (typically within a day) and without the limitations from adjusting the surface chemistry. Furthermore, plasmonic properties in macroscopic objects could be demonstrated for cryogelated aerogels [30].

In this work we investigate the impact of assembling nanoparticles into macroscopic monolithic aerogels using the cryogelation method. We concentrate on the

optical properties of Ag nanocrystal aerogels without a silica shell and with two differently thick silica shells to fabricate voluminous macroscopic aerogels with optical properties close to that of the colloidal solution. The reason to use Ag as plasmonic material results from its distinct and undisturbed LSPR. In contrast to Au nanopaticles, there is no spectral overlap between the LSPR and the electronic interband transition. Thus, occurring effects and changes in view of the plasmonic properties can be ascertained more easily. The nanoparticles are assembled either as micrometer thin aerogel films on glass supports or as macroscopic monolithic aerogels. By assembling the nanoparticles with tuned silica shell thicknesses, the Ag nanocrystals are brought into defined distances to each other. The aerogels are investigated for their optical properties as well as their morphology via spectroscopic and electron microscopical characterizations, respectively. Finally we discuss the sophisticated nature of the aerogel extinction spectra which are affected by a complex interplay of plasmon coupling and further optical effects.

2 Experimental section

2.1 Materials

Ethylene glycol (99%) was purchased from ABCR. Polyvinylpyrrolidone (Mw = 55,000, PVP), sodium hydroxide (>98%, NaOH), acetone (99%), (3-aminopropyl)trimethoxysilane (97%, APTMS), sulfuric acid (95–97 wt%, H_2SO_4) and ammonium hydroxide solution (28–30 wt%, NH_4OH) were purchased from Sigma Aldrich, Germany. Silver nitrate (99.85%, $AgNO_3$) was purchased from Acros. 2-propanol (99.5%), hydrogen peroxide (35 wt%, H_2O_2) and ethanol (99.8%) were purchased from Roth. Tetraethyl orthosilicate (>99.8%, TEOS) was purchased from Merck. All chemicals were used as received. Deionized water was used to disperse both the synthesized Ag nanocrystals and Ag–SiO_2 core-shell nanoheterostructures.

2.2 Synthesis of colloidal Ag nanocrystals

The colloidal Ag nanocrystals were synthesized according to the procedure of Zhang et al. [31]. Initially, 2.5 g PVP was dissolved under vigorous stirring in 200 mL ethylene glycol. Then 0.5 g $AgNO_3$ was added to the same solution. After the dissolution of the Ag precursor, the reaction mixture was heated up to 130 °C with a heating rate of around 7.4 °C/min and the reaction was allowed to

proceed for 90 min. When the solution has reached room temperature again, the Ag nanocrystals were precipitated by adding 800 mL acetone. Finally, the sample was separated from the reaction mixture employing centrifugation at 3773*g* for 15 min, followed by the redispersion in 40 mL deionized water.

2.3 Synthesis of colloidal Ag–SiO_2 core-shell nanoheterostructures

In order to grow a silica shell around the colloidal Ag nanoparticles, a procedure described by Zhang et al. [31] was employed. First of all, 7.52 mL of the in water dispersed Ag nanocrystals was dissolved in 80 mL isopropanol using an ultrasonic bath. Subsequently, the solution was stirred at 40 °C for 30 min, followed by the addition of 4 mL NH_4OH. After the temperature has stabilized, a specific TEOS amount was injected into the reaction mixture initiating the shell growth. The thickness of the silica shell could be controlled by the added quantity of the silica precursor. In this regard, the TEOS amount was 20 µL and 80 µL, respectively, in order to receive two different shell thicknesses. In total, the reaction was allowed to proceed under stirring for 2 h at 40 °C. Subsequently, the resultant nanoheterostructures were washed several times with water and ethanol. Finally, the Ag–SiO_2 core-shell nanoheterostructures were redispersed in 4 mL deionized water.

2.4 Synthesis of cryogelated aerogels

As previously reported by us for the gelation of other nanoparticles [30], the colloidal solutions were initially washed by means of a centrifuge filter (Merck Millipore, 10 kDa regenerated cellulose membrane) and concentrated up to a nanoparticle volume fraction of around 0.3%. For the fabrication of cryogelated aerogel films on a substrate, we first prepared glass supports by cleaning with piranha acid (H_2SO_4:H_2O_2) and eventually functionalizing with 5 M NaOH or APTMS. Then the colloidal solution was brought on the substrate via doctor-blading and immediate dipping into liquid nitrogen. After 5 min in the liquid nitrogen bath the slide was brought into a freeze dryer (Christ, Alpha 1-2LD plus) for at least 4 h with a pressure of 0.025 mbar. To obtain different film thicknesses, different volumes of nanoparticle solution were poured into rectangular molds with a constant area. Prior to this, the molds on the glass slides were created using adhesive tape.

The aerogel monoliths were prepared by drop-wise addition of the concentrated colloid direct into liquid nitrogen stored in a 20 mL vial. After storing it for around 10 min in liquid nitrogen, the complete sample vial was placed inside a freeze dryer for at least 24 h with a pressure of 0.025 mbar.

2.5 Optical characterization

The UV-VIS extinction spectra of the colloidal solutions were measured in a 3 mL quartz cuvette with a path length of 10 mm in transmission mode using a Cary 5000 spectrophotometer from Agilent Technologies. Absorption measurements were recorded with the same spectrophotometer equipped with an Agilent DRA-2500 integrating sphere and the cuvette in center-mount position. For the measurements of the nanoparticles, 5 µL of the as synthesized colloids were diluted with 3 mL deionized water. The thin aerogel films and aerogel monoliths were measured using a solid sample holder for the aerogel films and a 1 mL quartz cuvette filled with air and a path length of 4 mm for the monoliths, respectively. The scattering spectrum of the colloidal Ag nanocrystals was calculated by subtracting the absorption spectrum form the extinction spectrum.

2.6 Scanning electron microscope analysis

The samples were measured with an electron microscope JEOL JFM 6700F operating at 2 kV. Samples were prepared by placing small pieces onto an adhesive polymer carbon pod on top of the sample holder.

2.7 Transmission electron microscope analysis

TEM analyses were performed by means of a FEI Tecnai G2 F20 microscope, equipped with a field emission gun operated at 200 kV. For this purpose, the colloidal solutions were initially diluted with deionized water and then dropped on a carbon coated copper grid (Quantifoil, 300 mesh). In the case of aerogels, the grid was carefully pressed several times against the sample.

3 Results and discussion

3.1 Synthesis and characterization of Ag and Ag-SiO_2 nanoparticles

First of all, a solution of spherical Ag nanocrystals was synthesized according to the method reported by Zhang et al. as described in Section 2 [31]. Here, Ag^+ ions were reduced by ethylene glycol in the presence of polyvinylpyrrolidone (PVP) at

high temperatures producing nanoparticles with a mean diameter of 68 ± 12 nm (Figure S1A, Supporting Information). The benefits of this synthesis are the simple scalability and the high quantity of nanoparticles, which are essential for the preparation of aerogels by lyophilization. As can be seen from the UV-VIS spectrum (Figure 1a, black curve), the sample exhibits an increased extinction in the wavelength regime from 350 nm to 500 nm with a maximum at 415 nm. This characteristic feature of nanoscaled Ag is ascribed to the occurrence of the so-called LSPR and results from the resonant density oscillation of the conduction band electrons. It is known, that Ag nanocrystals undergo surface oxidation under aerobic conditions [32]. Therefore, the plasmonic properties should be generally influenced by a silver oxide layer in this work. Concerning this matter, the

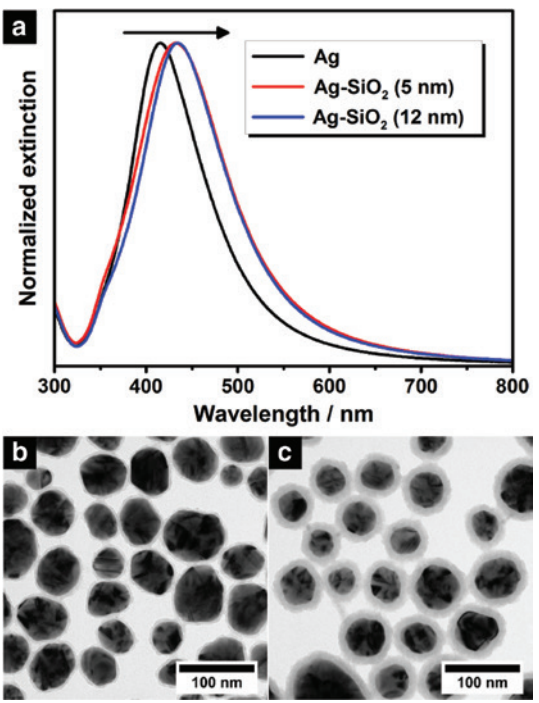

Fig. 1: Normalized extinction spectra (a) of colloidal Ag nanocrystals (black curve) and colloidal Ag–SiO_2 core-shell nanoheterostructures possessing a silica shell thickness of 5 nm (red curve) and 12 nm (blue curve), respectively. The measurements were performed in water for all samples. The arrow indicates the shift to longer wavelengths after the shell growth. The lower part shows the corresponding transmission electron microscope (TEM) images of the colloidal Ag–SiO_2 nanoheterostructures with a shell thickness of 5 nm (b) and 12 nm (c).

impact is expected to be revealed in a broadening and a shift of the LSPR peak. In addition to the absorption, resonant scattering contributes increasingly to the LSPR as expected for this size regime (Figure S1C, Supporting Information). In the case of small Ag nanocrystals with a radius less than 15 nm absorption entirely dominates their optical properties [33]. However, the scattering rises drastically with increasing nanoparticle size and eventually becomes the prevailing component due to its r^6 dependency (r being the radius), while the absorption efficiency scales only with r^3 [34].

After synthesizing spherical Ag nanocrystals, these particles were coated with a defined silica shell which is supposed to act as spacer material [31]. Following the Stöber method, the Ag nanocrystals were dispersed in isopropanol and treated with tetraethyl orthosilicate (TEOS) under alkaline conditions to accelerate the shell growth. In contrast to the often used citrate ligand, PVP ensures the stabilization of nanoparticles without any aggregation in alcohols and additionally promotes the silica coating [35]. By changing the TEOS amount, the shell thickness can be adjusted precisely, whereby the distance d between the surfaces of the adjacent Ag cores is finally determined in the three-dimensional aerogels (Figure 2d). For the following investigation two different shell thicknesses plus pure Ag nanocrystals without silica were employed. The corresponding transmission electron microscope (TEM) images of the colloidal Ag-SiO_2

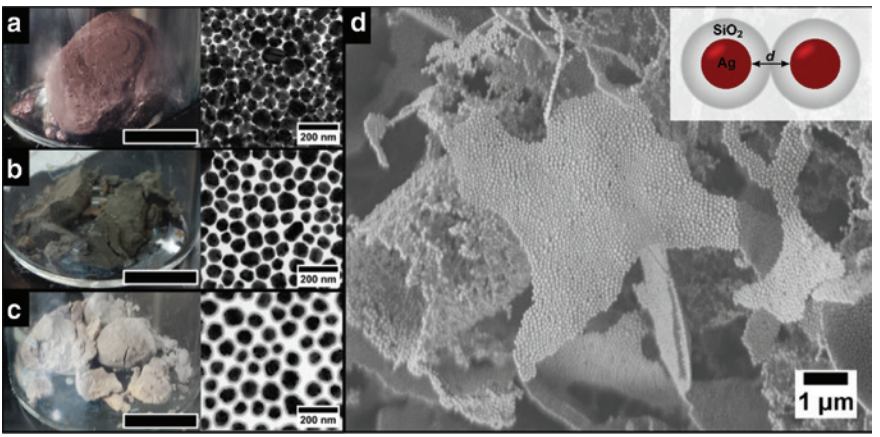

Fig. 2: Photographs and TEM images of cryogelated Ag aerogels without silica shell (a), with a 5 nm silica shell (b) and a 12 nm silica shell (c). The black bar represents 1 cm. Scanning electron microscope image (d) reveals the microscopic morphology of interconnected, one layer thin sheets build from the Ag nanoparticles with a 12 nm silica shell. The inset shows a scheme of two connected nanoparticles.

core-shell nanoheterostructures are illustrated in Figure 1b and c. As can be seen, by means of the Stöber method a uniform coating around the Ag nanocrystals was realized, with a thickness of 4.6 ± 0.8 nm and 12.0 ± 1.5 nm, respectively. The Ag cores of both nanoheterostructures exhibit a diameter of around 55 nm with a standard deviation of 13 nm in each case. Moreover, it should be noted, that no multi-core nanoheterostructures were observed; indeed each nanoparticle contains a single Ag core. Regarding the plasmonic properties, the LSPR of the colloidal Ag-SiO_2 nanoheterostructures is slightly shifted to longer wavelengths (bathochromic shift) compared to the one of the starting material (Figure 1a). This spectral displacement is expected for silica coatings due to the alteration of the refractive index of the surrounding medium. Generally, the LSPR wavelength and the refractive index of the medium exhibit a proportional relationship in the spectral range addressed here [36]. The change of the surrounding from water to silica leads to an increase of the refractive index at the particle surface from 1.33 to about 1.48 [37, 38]. Consequently, a bathochromic shift is both expected and observed. Another effect, which is associated with the change of the refractive index, concerns the linewidth of the LSPR. As investigated by Hu et al. [39], the increase of the refractive index causes a stronger radiative damping for the Ag nanocrystals. As a result, the linewidth of the LSPR broadens, which was also noticed for the Ag–SiO_2 nanoheterostructures. Despite a possibly formed silver oxide layer the silica shell seems thus to play a major role for the plasmonic properties.

3.2 Fabrication and characterization of Ag and Ag-SiO_2 cryogelated aerogel monoliths and thin films

3.2.1 SEM and TEM characterization

To fabricate cryogelated aerogel monoliths the colloidal solutions were concentrated and the solutions were injected dropwise into a vial filled with liquid nitrogen. Afterwards, the frozen colloidal solutions were transferred into a lyophilizer and freeze dried for 24 h. During the freezing of the colloids, the nanoparticles are not incorporated in the ice crystals but pushed into the voids between the ice crystals, if the ice growth velocity is high enough. In this way the building blocks are assembled into sheet-like structures, consisting of approximately 1–4 layers of nanoparticles, which are interconnected with each other and randomly oriented (Figure 2d) hence building up the macroscopic monoliths. A more detailed explanation on the formation mechanism can be found in our earlier work [30]. Simplified, the resulting monoliths can be described as randomly oriented two-dimensional sheets building a three-dimensional structure. The resulting aerogel

monoliths are highly voluminous and have an estimated density of around 0.03 g cm^{-1} (find the density estimation in Figure S3 in the supporting information – for drying at ambient conditions see supporting information Figure S4), which corresponds to a relative density of around 0.3% of the bulk Ag (for the cryogelated aerogel with no silica shell). The porosity is calculated to 99.7% with a pore size between the sheets in the micrometer range, while the pores within the sheets are nanometer sized. It can be seen from the photographs in Figure 2 that the cryogelated monoliths can be distinguished already by their macroscopic appearance. The aerogel composed of bare Ag nanocrystals has a reddish to violet appearance (Figure 2a) and in the case of the Ag nanocrystals with a 5 nm shell, the monolith exhibits a green grayish color (Figure 2b). The monolith made out of Ag cores with a 12 nm silica shell shows a yellow brownish color (Figure 2c), which is similar to that of the starting colloidal solution. As will be discussed later, this change in appearance is attributed to an interplay of various optical effects whose contributions depend on the employed building blocks. Generally, it is worth mentioning, that plasmonic properties could be conserved and influenced by the silica shell thickness in these macroscopic structures, which was not shown before [40].

For the fabrication of cryogelated aerogel films the colloidal solutions were brought on glass substrates via doctor-blading and immediate dipping into liquid nitrogen. Subsequently, the frozen films were dried within a lyophilizer for about 1 h. We observed similar effects for the thin aerogel films immobilized on glass substrates as for the monoliths (Figure 3a–c). Again nanoparticles are assembled into thin sheets forming an interconnected network (Figure 3e). However, when immobilized on a substrate the sheets have a preferred orientation standing mostly perpendicular on the substrate (Figure 3d). This observation can be explained by the temperature gradient while dipping the glass in liquid nitrogen. The technique of aligning structures by an applied temperature gradient is known as directed freezing and was also exploited in our earlier work [30, 41]. Similar as in the case of monoliths, the aerogel films have distinct optical appearances resulting from the same mechanisms occurring in the monoliths. Further SEM and TEM images of the fabricated aerogel monoliths and films can be found in Figures S5 to S10 of the Supporting Information.

3.2.2 Optical properties of cryogelated aerogel films and monoliths

The last part of this work focuses on the optical properties of these three-dimensional nanoparticle aerogels. The monoliths could only be characterized in terms of their optical properties by means of reflectance measurements, since their volume is too big for transmission experiments. Therefore, we concentrate on the

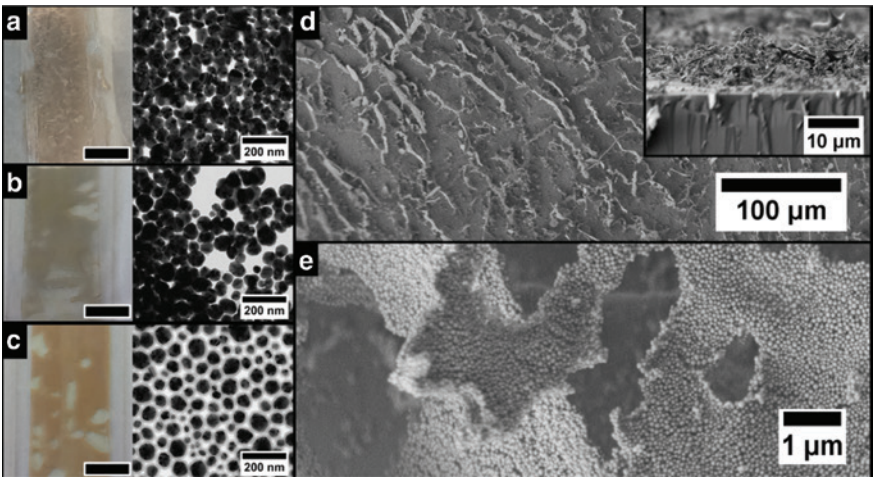

Fig. 3: Photographs and TEM images of doctor-bladed cryogelated Ag aerogel films on a glass substrate without silica shell (a), with a 5 nm silica shell (b) and with a 12 nm silica shell (c). The black bar represents 1 cm. Scanning electron microscope image (d) reveals that the nanoparticle sheets preferably stand perpendicular on the substrate. As can be seen in the inset the thickness of the film is approximately 10 µm. The sheets itself are again build from Ag nanoparticles with a 12 nm silica shell (e) similar to the monolithic aerogels.

aerogel films as in contrast to the monoliths they were optically characterized by both extinction and absorption measurements. To ensure a better comparability, the UV-VIS spectra of the cryogelated aerogel films as well as of the related colloidal solutions are presented in Figure 4.

In the case of the pure Ag aerogel film, the extinction spectrum (Figure 4a, red solid curve) exhibits two bands whose maxima are located around 403 nm and 657 nm, respectively. Due to its spectral position we attribute the short-wavelength peak to LSPR excitation in the nanoparticles. We conjecture that the reason for its rather pronounced appearance is the coverage of the Ag nanocrystals by insulating PVP ligands from the synthesis which hampers electronic interparticle transport. Hence, the short-wavelength peak represents optical features of single particles in the spectrum. However, their assembly to aerogel film induces a strong LSPR broadening and a spectral shift of 12 nm to shorter wavelengths (hypsochromic shift) compared to the one of the colloidal solution (Figure 4a, solid curves).

The corresponding absorption spectrum of the same sample (Figure 4a, red dashed curve) reveals a further interesting finding. In contrast to the extinction graph, the long-wavelength band has vanished and instead a small shoulder at around 590 nm can be noticed. The shape difference between the extinction and the absorption spectra in the long-wavelength range leads us to the conclusion

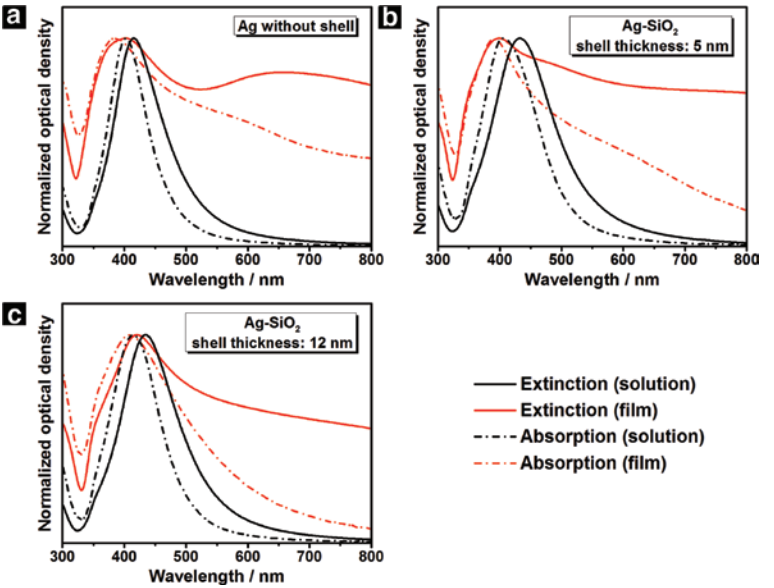

Fig. 4: Normalized extinction (solid line) and normalized absorption (dashed line) spectra of the cryogelated aerogel films (red curve) as well as the corresponding colloidal solution (black curve): Ag (a) as well as Ag–SiO_2 with a shell thickness of 5 nm (b) and 12 nm (c).

that besides LSPR excitation further optical effects play a role which mainly contribute via scattering or reflection. Possible effects include the excitation of propagating surface plasmons in the aerogel sheets, scattering effects due to the surface roughness induced by depositing the material on the glass surface (see Figure 3d), and the formation of an effective medium formed from Ag and air the effective refractive index of which may lead to spectrally inhomogeneous reflection. The shape differences between the extinction and absorption spectra are also found for the aerogels consisting of Ag particles carrying a silica shell (Figure 4b and c). The thickness of the aerogel films appeared to have no influence on the shape of the optical spectra but only on their optical density (Figure S11).

Both a precise understanding of the interplay of the abovementioned effects as well as a simulation of the optical properties of the complex surface structures is beyond the scope of this paper. However, we will discuss the behavior of the short-wavelength peak as this can clearly be attributed to single-particle LSPR origin and its conservation during aerogel formation is the aim of this work. Generally, two tendencies become apparent by comparing the spectra of the three aerogel films (Figure 5): While the extinction in the long-wavelength part of the spectrum decreases with increasing silica shell thickness, the LSPR peak exhibits a bathochromic shift. In other words, an increasing shell thickness leads to an

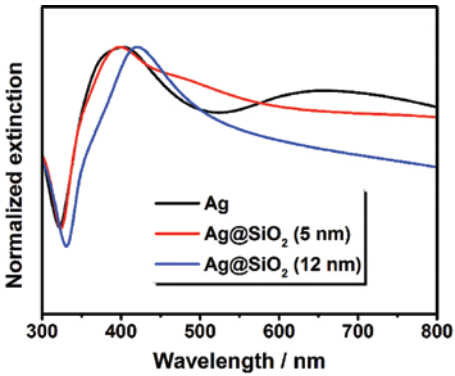

Fig. 5: Normalized extinction spectra of the cryogelated aerogel films: Ag (black curve) as well as Ag–SiO_2 with a shell thickness of 5 nm (red curve) and 12 nm (blue curve).

increasing similarity between the optical properties of the colloidal particles and the aerogels.

The spectral shift of the broadening of the short-wavelength peak can be explained as follows: In contrast to the colloidal solution, the individual nanocrystals in such assemblies are in direct contact with each other. As a result of this, the plasmon oscillations of the individual Ag nanocrystals can strongly interact with each other, which is known as plasmon coupling. The efficiency of the coupling depends on the distance between the plasmonic cores defined in this case by the silica shell thickness. An established explanation of the mechanism is provided by the plasmon hybridization theory. Fundamentally, the plasmon coupling is based on electrostatic dipolar interactions leading to a spectral shift and a broadened linewidth of the LSPR. In literature, there are several works concerning the mechanism in detail. Here, an established explanation is provided by the plasmon hybridization theory [42–44]. In this regard, the coupling depends on the arrangement of the plasmonic nanoparticles. For example, Brandle et al. [43] have investigated the plasmonic properties of trimers and quadrumers. With regard to our work, a detailed coupling mechanism cannot be currently stated due to the complex structure of the aerogels. However, the sheet-like arrangement of the Ag nanocrystals seems to induce a coupling resulting in an increase of the LSPR excitation energy. In line with the theory the bathochromic shift of the LSPR peak with increasing silica shell thickness indicates a weakening of the plasmon coupling. Consequently, the aerogel with a 12 nm silica shell exhibits a LSPR which resembles the one of the corresponding colloidal solution. Finally it should be noted, that the observed behavior is uncommon. Several works report on a decrease of the LSPR excitation energy in association with the plasmon coupling.

To summarize, the investigation of the Ag and Ag–SiO_2 aerogel films have revealed that the optical properties originate from different mechanisms. In this context, the degree of plasmon coupling as well as the occurrence of further optical effects greatly depends on the interparticle distance defined by the silica shell thickness. While a shell thickness of 12 nm leads to optical properties similar to the ones of the colloidal solution, the bare Ag aerogel film spectrum is heavily distorted in comparison to the colloidal case. Finally we turn to a discussion of the optical properties of the cryogelated monoliths. As can be seen from the reflectance spectra (Figure S12, Supporting Information), the spectral signature of all samples possesses a minimum at 324 nm, which becomes more defined with decreasing silica shell thickness [45]. This feature is ascribed to the so-called plasma edge and typically appears in the reflectance spectra of bulk materials. In comparison with the aerogel films, the processes affecting the optical properties in these structures are considerably more complex and not easy to explain due to the irregular arrangement of the sheet-like structural units. However, the same tendency becomes apparent like in the case of the aerogel films, by considering the development of the plasma edge. This means, that the optical properties of the monoliths more and more resemble the behavior of a bulk material with decreasing silica shell thickness.

4 Conclusion

In summary this work shows the fabrication of macroscopic, porous and voluminous Ag nanoparticle structures with plasmonic characteristics conserved in the final object. Our method is faster and less complex compared to hydrogelated aerogels. While the assembly does not modify the Ag nanocrystals, predominantly plasmonic coupling occurs in dependence of the interparticle distance. These distances – and hence the optical properties of the aerogels – can be controlled and adjusted by employing silica shells of varying thickness. Concluding, we were able to demonstrate the fabrication of macroscopic aerogels with retained nanoscopic plasmonic properties, which could not be shown with other methods so far.

5 Supporting information

TEM images of the Ag nanocrystals, size distribution of the Ag nanocrystals as well as the silica shell thickness, further UV-VIS spectra and further SEM images of the aerogels.

Acknowledgements: T. K. and D. D. want to thank the German research foundation (DFG, research grants DO1580/2-1 and DO1580/3-1) for funding. A. F., S. N. and N. C. B. are thankful for the financial support to German Ministry of Education and research (BMBF, NanoMatFutur, support code 03X5525). For the funding from the European Research Council (Horizon 2020, grant agreement No 714429/ERC Starting Grant MAEROSTRUC) the N. C. B. is also grateful. Moreover, T. K. and A. S. are grateful to the Hannover School for Nanotechnology (hsn) for the financial support.

References

1. G. Mie, Ann. Phys. **330** (1908) 377.
2. H. Siedentopf, R. Zsigmondy, Ann. Phys. **10** (1903) 1.
3. C. Sönnichsen, B. M. Reinhard, J. Liphardt, A. P. Alivisatos, Nat. Biotechnol. **23** (2005) 741.
4. W. R. Holland, D. G. Hall, Phys. Rev. B **27** (1983) 7765.
5. L. Wu, B. M. Reinhard, Chem. Soc. Rev. **43** (2014) 3884.
6. C. J. Murphy, T. K. Sau, A. M. Gole, C. J. Orendorff, J. Gao, L. Gou, S. E. Hunyadi, T. Li, J. Phys. Chem. B **109** (2005) 13857.
7. L. M. Liz-Marzán, M. Giersig, P. Mulvaney, Langmuir **12** (1996) 4329.
8. N. C. Bigall, T. Härtling, M. Klose, P. Simon, L. M. Eng, A. Eychmüller, Nano Lett. **8** (2008) 4588.
9. D. Dorfs, A. Eychmüller, Nano Lett. **1** (2001) 663.
10. D. Dorfs, T. Härtling, K. Miszta, N. C. Bigall, M. R. Kim, A. Genovese, A. Falqui, M. Povia, L. Manna, J. Am. Chem. Soc. **133** (2011) 11175.
11. D. D. Smith, L. A. Snow, L. Sibille, E. Ignont, J. Non Cryst. Solids **285** (2001) 256.
12. A. Tao, P. Sinsermsuksakul, P. Yang, Nat. Nanotechnol. **2** (2007) 435.
13. P. K. Jain, M. A. El-Sayed, Chem. Phys. Lett. **487** (2010) 153.
14. N. J. Halas, S. Lal, W.-S. Chang, S. Link, P. Nordlander, Chem. Rev. **111** (2011) 3913.
15. S. K. Ghosh, T. Pal, Chem. Rev. **107** (2007) 4797.
16. J. A. Jenkins, Y. Zhou, S. Thota, X. Tian, X. Zhao, S. Zou, J. Zhao, J. Phys. Chem. C **118** (2014) 26276.
17. P. K. Jain, X. Huang, I. H. El-Sayed, M. A. El-Sayed, Acc. Chem. Res. **41** (2008) 1578.
18. M. Rycenga, C. M. Cobley, J. Zeng, W. Li, C. H. Moran, Q. Zhang, D. Qin, Y. Xia, Chem. Rev. **111** (2011) 3669.
19. J. Gong, G. Li, Z. Tang, Nano Today **7** (2012) 564.
20. S. Sánchez-Paradinas, D. Dorfs, S. Friebe, A. Freytag, A. Wolf, N. C. Bigall, Adv. Mater. **27** (2015) 6152.
21. S. Naskar, J. F. Miethe, S. Sánchez-Paradinas, N. Schmidt, K. Kanthasamy, P. Behrens, H. Pfnür, N. C. Bigall, Chem. Mater. **28** (2016) 2089.
22. S. S. Kistler, Nature **127** (1931) 741.
23. N. Hüsing, U. Schubert, Angew. Chem. Int. Ed. **37** (1998) 22.
24. J. L. Mohanan, I. U. Arachchige, S. L. Brock, Science **307** (2005) 397.
25. A. Eychmüller, Angew. Chem. Int. Ed. **44** (2005) 4839.

26. N. C. Bigall, A.-K. Herrmann, M. Vogel, M. Rose, P. Simon, W. Carrillo-Cabrera, D. Dorfs, S. Kaskel, N. Gaponik, A. Eychmüller, Angew. Chem. Int. Ed. **48** (2009) 9731.
27. S. L. Brock, I. U. Arachchige, K. K. Kalebaila, Comments Inorg. Chem. **27** (2006) 103.
28. A.-K. Herrmann, N. C. Bigall, L. Lu, A. Eychmüller, Ordered and Nonordered Porous Superstructures from Metal Nanoparticles, Wiley-VCH Verlag GmbH & Co. KGaA, Weinheim (2012), pp. 339–359.
29. A.-K. Herrmann, W. Liu, N. Gaponik, N. C. Bigall, A. Eychmuller, ECS Trans. **45** (2013) 149.
30. A. Freytag, S. Sánchez-Paradinas, S. Naskar, N. Wendt, M. Colombo, G. Pugliese, J. Poppe, C. Demirci, I. Kretschmer, D. W. Bahnemann, P. Behrens, N. C. Bigall, Angew. Chem. Int. Ed. **55** (2016) 1200.
31. F. Zhang, G. B. Braun, Y. Shi, Y. Zhang, X. Sun, N. O. Reich, D. Zhao, G. Stucky, J. Am. Chem. Soc. **132** (2010) 2850.
32. A. Henglein, Chem. Mater. **10** (1998) 444.
33. D. D. Evanoff Jr., G. Chumanov, J. Phys. Chem. B **108** (2004) 13957.
34. C. F. Bohren, D. R. Huffman, Absorption and Scattering of Light by Small Particles, Wiley, New York (1983).
35. C. Graf, D. L. J. Vossen, A. Imhof, A. van Blaaderen, Langmuir **19** (2003) 6693.
36. U. Kreibig, M. Vollmer, Optical properties of metal clusters, Vol. 25, Springer series in materials science, Springer, Berlin, Heidelberg (1995).
37. B. N. Khlebtsov, V. A. Khanadeev, N. G. Khlebtsov, Langmuir **24** (2008) 8964.
38. G. M. Hale, M. R. Querry, Appl. Opt. **12** (1973) 555.
39. M. Hu, C. Novo, A. Funston, H. Wang, H. Staleva, S. Zou, P. Mulvaney, Y. Xia, G. V. Hartland, J. Mater. Chem. **18** (2008) 1949.
40. X. Gao, R. J. Esteves, T. T. H. Luong, R. Jaini, I. U. Arachchige, J. Am. Chem. Soc. **136** (2014) 7993.
41. L. Qian, H. Zhang, J. Chem. Technol. Biotechnol. **86** (2011) 172.
42. P. Nordlander, C. Oubre, E. Prodan, K. Li, M. I. Stockman, Nano Lett. **4** (2004) 899.
43. D. W. Brandl, N. A. Mirin, P. Nordlander, J. Phys. Chem. B **110** (2006) 12302.
44. E. Prodan, C. Radloff, N. J. Halas, P. Nordlander, Science **302** (2003) 419.
45. J. Springer, A. Poruba, L. Müllerova, M. Vanecek, O. Kluth, B. Rech, J. Appl. Phys. **95** (2004) 1427.

Supplementary Material: The online version of this article offers supplementary material (https://doi.org/10.1515/zpch-2017-1045).